Laser and Particle Beams (2006), *24*, 223–230. Printed in the USA.

DOI: 10.1017/S0263034606060320

Stochastic heating in ultra high intensity laser-plasma interaction: Theory and PIC code simulations

D. PATIN, E. LEFEBVRE, A. BOURDIER, AND E. D'HUMIÈRES

Commissariat l'Energie Atomique, DAM-Lle de France, Département de Physique Théorique et Appliquée, Bruyéres-le-Châtel, France

(RECEIVED 28 October 2005; ACCEPTED 22 December 2005)

Abstract

In the first part, the theoretical model of the stochastic heating effect is presented briefly. Then, a numerical resolution of the Hamilton equations highlights the threshold of the stochastic effect. Finally, Particle-In-Cell (PIC) code simulations results, for experimentally relevant parameters, are presented in order to confirm the acceleration mechanism predicted by the one-particle theoretical model. This paper gives the conditions on the different experimental parameters in order to have an optimization of the stochastic heating.

Keywords: Laser-plasma interaction; PIC code; Stochastic heating

1. INTRODUCTION

A large number of issues remain open in the study of laser-matter interaction at very high intensities. Recently, PIC code simulations results published by Tajima *et al.* show that the irradiation of very high intensity lasers on clustered matter leads to a very efficient heating of electrons (Tajima *et al.*, 2001). They have shown that chaos seems to be the origin of the strong laser coupling with clusters. The existence of stochastic heating was recently confirmed (Bourdier *et al.*, 2005; Sheng *et al.*, 2002, 2004; Bourdier & Patin, 2005; Patin *et al.*, 2005). Therefore, the issue that we will address in this paper is the stability of electron motion in the fields of several waves. We studied this motion in a high intensity plane wave, perturbed by one or two electromagnetic plane waves. The solution of Hamilton-Jacobi equation is used to identify resonances. Above the Chirikov threshold, and for electron trajectories with their initial conditions in the phase-space region where resonances overlap, stochastic heating is evidenced by computing single particle energy. This paper gives new results in the sense that the two counter propagating waves is not the most efficient system for the stochastic heating. Then, PIC code simulations results obtained with the code CALDER are presented in order to validate the theoretical model for experimentally relevant parameters. A significant enhancement of laser absorption is observed for parameters where stochastic heating is expected. The influence of the plasma density and the ratio of the amplitude of the two counter propagating laser pulses on the stochastic effect is evaluated.

Address correspondence and reprint requests to: David Patin, Commissariat l'Energie Atomique, DAM-Lle de France, Département de Physique Théorique et Appliquée, BP 12, 91680 Bruyéres-le-Châtel, France. E-mail: david.patin@pgp.u-psud.fr

2. THEORETICAL MODEL FOR THE ONSET OF STOCHASTIC HEATING

2.1. Hamiltonian formulation of the system

A charged particle interacting with two electromagnetic planes waves is considered. One has a high intensity:

$$\vec{a}_0(\vec{r},t) = a_0 \cos(t-z)\vec{e}_x, \tag{1}$$

and the second, perturbing wave, a_1, is in the same polarization plane propagating at some angle α with respect to a_0 ($a_1 \ll a_0$):

$$\vec{a}_1(\vec{r},t) = a_1[\sin\alpha\vec{e}_z - \cos\alpha\vec{e}_x]\sin(\omega_1 t - k_\parallel z - k_\perp x), \tag{2}$$

with $k_\parallel = k_1\cos\alpha$ and $k_\perp = k_1\sin\alpha$, where $k_1 = \|\vec{k}_1\|$. In the following we will use $e = m = c = 1$.

The Hamiltonian of an electron interacting with both the $\vec{a}_0$ and $\vec{a}_1$ waves is:

$$H(\vec{r},t,\vec{P},-\gamma) = 1 + [\vec{P} + \vec{a}_0(\vec{r},t) + \vec{a}_1(\vec{r},t)]^2 - \gamma^2. \tag{3}$$

We rewrite H as $H = H_0 + H_1$, where H_0 is the integrable part of the Hamiltonian and H_1 is the perturbation. In order to write H in the action-angle variables of H_0, we used the relations (Bourdier *et al.*, 2005; Bourdier & Patin, 2005; Patin *et al.*, 2005; Rax, 1992):

$$x = \theta + \frac{a}{P_\parallel - E}\sin(\phi + \varphi), \tag{4}$$

$$z = \varphi - \frac{P_\perp}{(P_\parallel - E)^2}\, a\sin(\phi + \varphi) - \frac{a^2}{8(P_\parallel - E)^2}\sin(2(\phi + \varphi)), \tag{5}$$

$$t = -\phi - \frac{P_\perp}{(P_\parallel - E)^2}\, a\sin(\phi + \varphi) - \frac{a^2}{8(P_\parallel - E)^2}\sin(2(\phi + \varphi)), \tag{6}$$

$$p_x = P_\perp + a\cos(\phi + \varphi), \tag{7}$$

$$p_z = P_\parallel - \frac{P_\perp}{P_\parallel - E}\, a\cos(\phi + \varphi) - \frac{a^2}{4(P_\parallel - E)}\cos(2(\phi + \varphi)), \tag{8}$$

$$\gamma = E - \frac{P_\perp}{P_\parallel - E}\, a\cos(\phi + \varphi) - \frac{a^2}{4(P_\parallel - E)}\cos(2(\phi + \varphi)), \tag{9}$$

where p_x (resp. p_z) is the normalized momentum along the x-axes (resp. z-axes), and H_1 expressed in terms of the action angle variables $(P_\perp, P_\parallel, E, \theta, \varphi, \phi)$ of H_0 (Rax, 1992).

We can notice that $P_\perp = \langle p_x \rangle$, $P_\parallel = \langle p_z \rangle$ and $E = \langle \gamma \rangle$.

One has:

$$H_0(P_\perp, P_\parallel, E) = 1 + \frac{a_0^2}{2} + P_\perp^2 + P_\parallel^2 - E^2. \tag{10}$$

Neglecting the a_1^2 term:

$$H_1(P_\perp, P_\parallel, E, \theta, \varphi, \phi) = a_1 \sum_N V_N \cos[k_\parallel \varphi + k_\perp \theta + \omega_1 \phi + N(\varphi + \phi)], \tag{11}$$

where $V_N = V_N(P_\perp, P_\parallel, E)$ is the amplitude of the Nth resonant term.

2.2. Resonance condition and stochasticity threshold

The resonance condition is found by using the standard perturbation technics (Tajima *et al.*, 2001; Patin *et al.*, 2005; Rax, 1992):

$$k_\parallel P_\parallel + k_\perp P_\perp - \omega_1 E - N(E - P_\parallel) = 0. \tag{12}$$

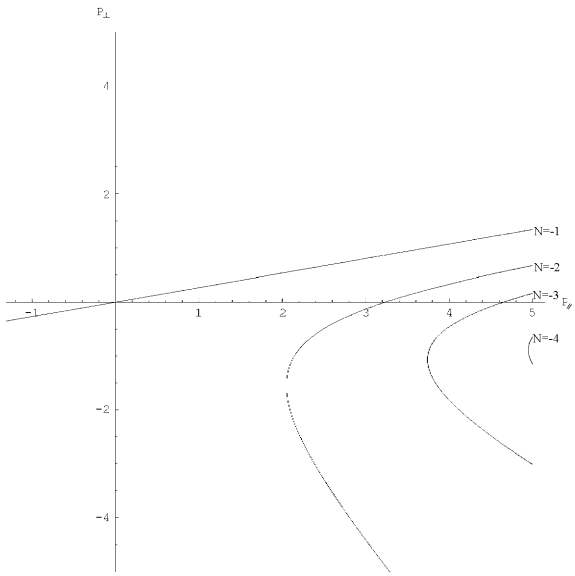

Fig. 1. Resonance in the $(P_\parallel, P_\perp)$ plane, $a_0 = 2$, $\omega_1 = k_1 = 1$ and $\alpha = \pi/6$.

As $H_0 = 0$, one has:

$$E(P_\perp, P_\parallel) = \sqrt{1 + \frac{a_0^2}{2} + P_\perp^2 + P_\parallel^2}\quad . \tag{13}$$

Using this equation and Eq. (12) allows to calculate $P_\perp$ versus $P_\parallel$. Figure 1 displays the resonance lines for $\alpha = \pi/6$, and shows that these lines are quite far from each other in this case. Chaos will occur when the sum of th half-widths of two neighboring resonances, ΔJ, becomes larger than the distance between them, d. This condition is known as the Chirikov criterion (Chirikov, 1979):

$$R = \frac{\Delta J}{d} > 1. \tag{14}$$

We will show below that the resonance width is weakly dependant on the angle α. Therefore, we expect that chaos will set in easily if the resonance lines are closer, as is the case in Figure 2 for $\alpha = 5\pi/6$. In order to prove this assertion rigorously, we need to calculate the width of the resonance. Following Rax (1992) and Tabor (1989), the resonance width is given by:

$$\Delta J = 2\sqrt{\frac{a_1 |V_N|}{|k_\perp^2 + (k_\parallel + \omega_1 + 2N)|}}. \tag{15}$$

We note that ΔJ depends on α through its sine and cosine (remembering that $k_\parallel = k_1 \cos\alpha$ and $k_\perp = k_1 \sin\alpha$). So, the width of the resonance is not strongly dependent on α. Remembering that the aim is to have global stochasticity, we

https://doi.org/10.1017/S0263034606060320 Published online by Cambridge University Press

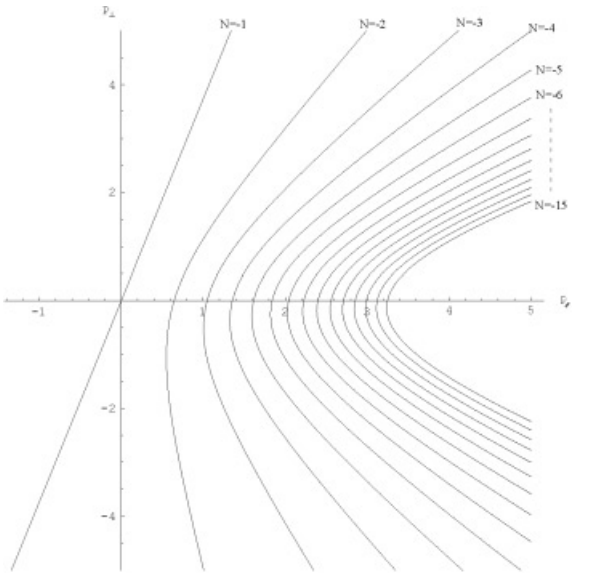

Fig. 2. Resonance in the $(P_{\parallel}, P_{\perp})$ plane, $a_0 = 2$, $\omega_1 = k_1 = 1$ and $\alpha = 5\pi/6$.

must find conditions such that the Chirikov criterion is satisfied as widely as possible.

First, we compute the Chirikov criterion parameter in the $\{\alpha;\omega_1\}$ space. Figures 3 and 4 display the region in the $\{\alpha;\omega_1\}$ space where $R > 1$. In other words, it is the region where the Chirikov criterion is satisfied and stochastic heating should be strong. Figures 3 and 4 are symmetric with respect to the $\alpha = \pi$ axis. Furthermore, the Chirikov criterion is satisfied when α is close to π and when ω_1 is in the range (Tajima *et al.*, 2001; Bourdier *et al.*, 2005).

It is also interesting to know the wave-intensity threshold for the stochastic effect. We can know this by plotting the Chirikov criterion parameter in the $\{a_0;a_1\}$ space, for given values of α and ω_1. We can see clearly in Figures 5 and 6 that there is a threshold in a_1 for the stochastic heating effect.

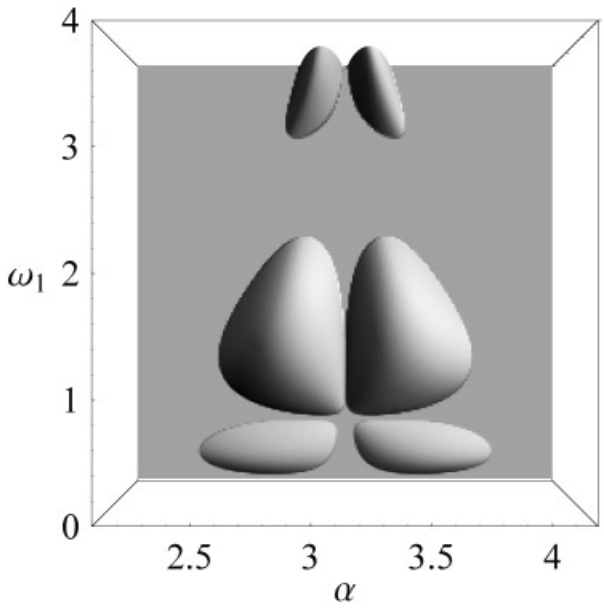

Fig. 4. Zone (view 2) (in the $(\alpha;\omega_1)$ space) where the Chirikov criterion is satisfied for resonances $N = -1; N = -2$ with $P_{\perp} = 0$; $a_0 = 1$ and $a_1 = 0.1$.

2.3. Numerical resolution of the theoretical model's equation

Several numerical results are presented in order to validate the theoretical hypothesis. First, we compare the particle energy in two different cases corresponding to an one-wave case, and a two-wave case. Figure 7 shows the particle energy versus the time calculated through the Hamiltonian one-particle model in the one-wave case. Figure 8 is for the two-wave case. In this last case, the particle has a chaotic motion, its average energy is higher due to the stochastic heating. It is also interesting to plot the behavior in the $(p_x;p_z)$ space. Figures 9 and 10 display the motion in the

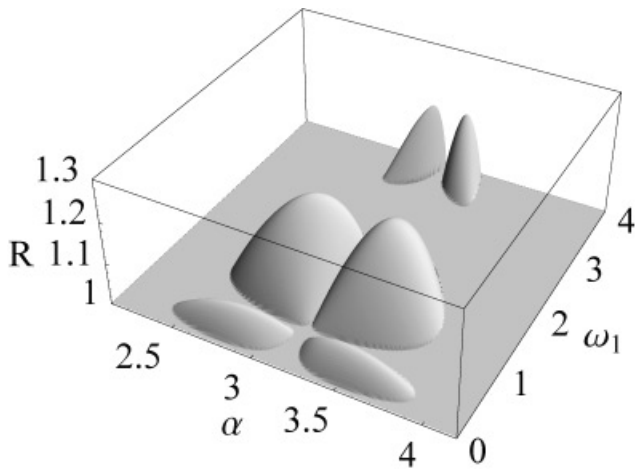

Fig. 3. Zone (view 1) (in the $(\alpha;\omega_1)$ space) where the Chirikov criterion is satisfied for resonances $N = -1; N = -2$ with $P_{\perp} = 0$; $a_0 = 1$ and $a_1 = 0.1$.

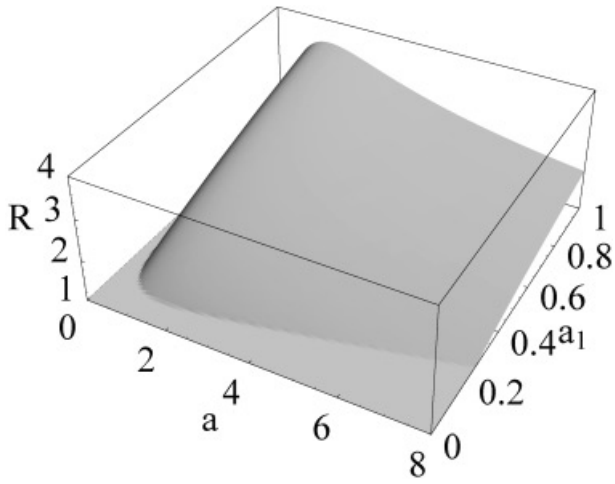

Fig. 5. Zone (view 1) (in the $(a_0;a_1)$ space) where the Chirikov criterion is satisfied for resonances $N = -1; N = -2$ with $P_{\perp} = 0$; $\omega_1 = 1$ and $\alpha = 5\pi/6$.

https://doi.org/10.1017/S0263034606060320 Published online by Cambridge University Press

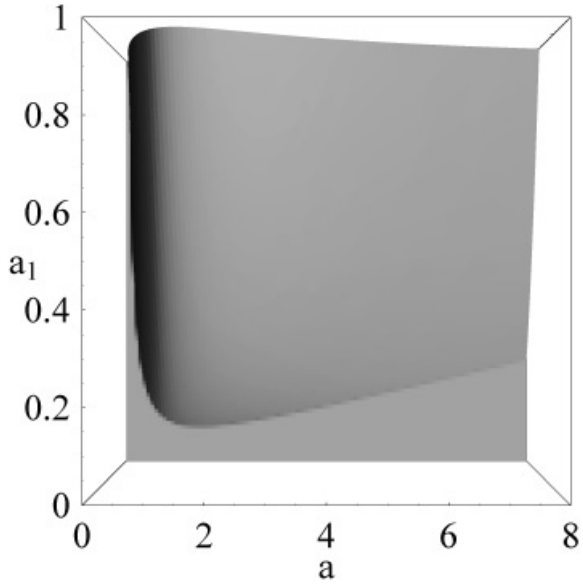

Fig. 6. Zone (view 2) (in the $(a_0;a_1)$ space) where the Chirikov criterion is satisfied for resonances $N=-1; N=-2$ with $P_\perp = 0$; $\omega_1 = 1$ and $\alpha = 5\pi/6$.

$(p_x;p_z)$ space. In the one-wave case (Fig. 9), the particle is in one resonance, whereas in Figure 10, the particle can travel from one resonance to another. Remembering that $P_\perp = \langle p_x \rangle$, $P_\parallel = \langle p_z \rangle$, we notice that the particle fills the resonance diagram (Fig. 2). Now, we can highlight the stochastic threshold in intensity by computing the motion in the $(p_x;p_z)$ space for two different values of a_1.

Figures 11 to 14 are all for two-waves cases. Figures 11 and 13 are for $a_1 = 0.2$. Figures 12 and 14 are for $a_1 = 0.3$. The difference is striking, with a very regular motion for the two-wave case at low perturbing wave intensity, and the expected chaotic behavior at larger value of a_1. It is explained by Figure 6. Indeed, in one case ($a_1 = 0.2$), the Chirikov criterion is not satisfied and, in the other case ($a_1 = 0.3$), the Chirikov criterion is satisfied. In consequence, the particle is free to pass from resonance to resonance and can reach higher energies.

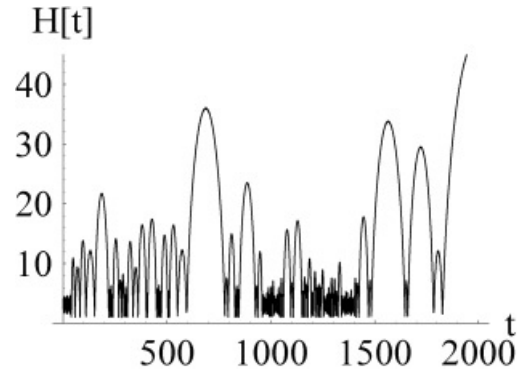

Fig. 8. Hamiltonian versus time in the two-wave case with $\alpha = 5\pi/6$, $\omega_1 = k_1 = 1$, $a_0 = 4.0$ and $a_1 = 0.4$.

3. PIC CODE SIMULATIONS

In order to assess the potential relevance of stochastic heating in realistic situations, we need to compare its importance with that of other laser-plasma interaction mechanisms. Particle-In-Cell (PIC) simulations are well suited for such a comparison. In this section, we use the CALDER code (Lefebvre *et al.*, 2003; Pommier & Lefebvre, 2003) to perform these simulations. CALDER is a massively parallel, multi-dimensional, and fully relativistic PIC code. It self-consistently solves Maxwell and Vlasov equations for the electromagnetic field and plasma electrons, respectively, and is therefore able to simultaneously model stochastic and collective absorption processes.

3.1. PIC simulation with one particle

Before addressing the interplay between collective and individual absorption mechanisms, we first wanted to make sure that the stochastic behavior was correctly modeled by the PIC code. We therefore started with simulations including a very-low-density plasma, with only one particle. Figure 15 displays the particle energy versus time in two cases. The black curve correspond to the one-wave case. As it is well

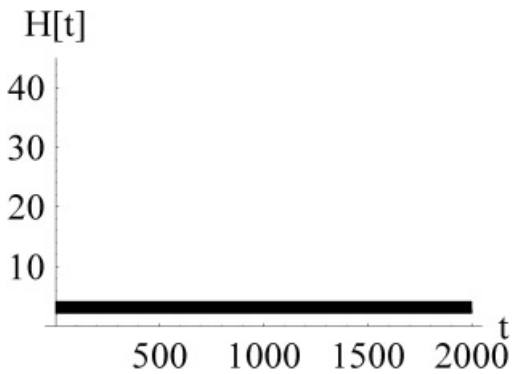

Fig. 7. Hamiltonian versus time in the one-wave case with $a_0 = 4.02$.

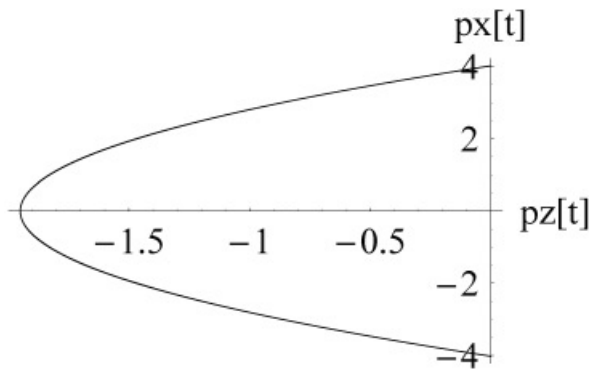

Fig. 9. Motion in the $(p_x;p_z)$ space in the one-wave case with $a_0 = 4.02$.

https://doi.org/10.1017/S0263034606060320 Published online by Cambridge University Press

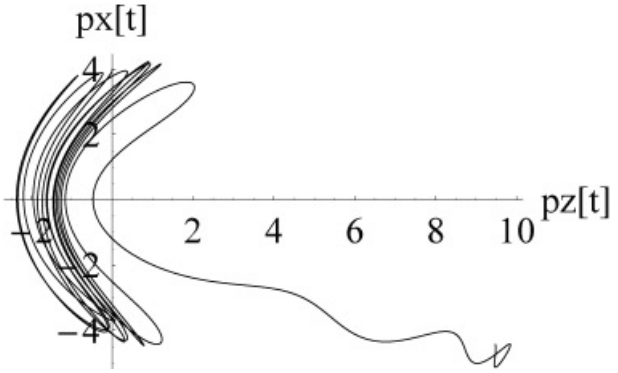

Fig. 10. Motion in the $(p_x; p_z)$ space in the two-wave case with $\alpha = 5\pi/6$, $\omega_1 = k_1 = 1$, $a_0 = 4.0$ and $a_1 = 0.4$.

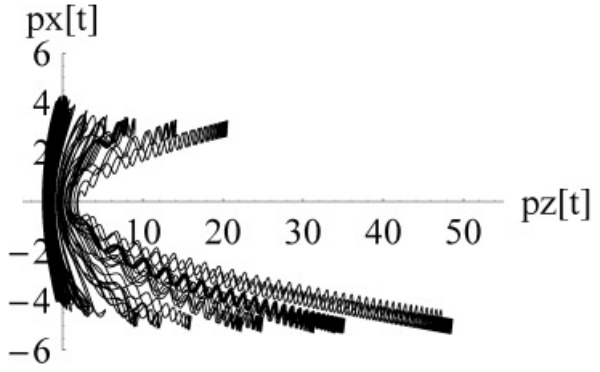

Fig. 12. Motion in the $(p_x; p_z)$ for $a_0 = 4$, $\omega_1 = 1$, $\alpha = 5\pi/6$ and $a_1 = 0.3$.

known, the energy oscillate in the electromagnetic wave. The red curve is for the two-wave case. In this case the energy curve has a chaotic behavior.

The Figures 8 and 15 are of the same type. The differences come from the fact that in the PIC code simulation we have a half-plane wave. So there is a discontinuity in the electromagnetic field; the particle undergoes a kick. The system is chaotic, as a consequence, a minor change in the initial conditions or in the value of the electromagnetic field changes the trajectories. Furthermore, the particle motion integrators in the PIC code and for the numerical resolution of Hamilton's equation are different. So it is not surprising that the details of the chaotic curves are different in Figures 8 and 15. Figure 16 displays the particle trajectory in the $(p_x; p_z)$ phase space computed with the PIC code. Again, the motion is absolutely similar to the one obtained in Figure 12.

3.2. Influence of the angle between the waves

To assess the relevance of stochastic heating in realistic situations, we performed a series of two-dimensional-simulation, where we have $a_0 = 1$ (amplitude of the high intensity wave), $a_1 = 0.1$ (amplitude of the perturbing wave), $\tau_0 = 0.60\ ps$ (last of the high intensity wave), $\tau_1 = 0.62\ ps$ (last of the perturbing wave), $T_{e,i} = 1\ keV$ (initial temperature of the electrons), and $n = 0.01\ n_c$ (density of the plasma). Figure 17 displays the evolution of the kinetic energy of the electrons when $\alpha = 5\pi/6$, $\alpha = \pi/6$, and $\alpha = 0$. It shows that the highest energy transferred to the electrons is when $\alpha = 5\pi/6$.

The energy of the electrons in the one-wave case is due to the ponderomotive force. In the other two cases, the ponderomotive effect still exists, but a new phenomenon takes place due to the stochastic heating effect. We can conclude two things. First, the stochastic heating mechanism can be readily observed with PIC code simulations. Then, the stochastic heating is shown to be more efficient when the waves are almost, but not exactly, counter propagating. According to the theoretical model, the Chirikov criterion is indeed achieved more easily when $\alpha = 5\pi/6$.

3.3. Influence of ω_1

In the next series of two-dimensional-simulations, the parameters are $a_0 = 3.922$, $a_1 = 0.784$, $n = 10^{-2} n_c$, $\tau_0 = \tau_1 = 0.3\ ps$, and $\alpha = 5\pi/6$. Figures 18 and 19 show that the gain is inversely proportional to ω_1. Indeed, Figures 3 and 4 show

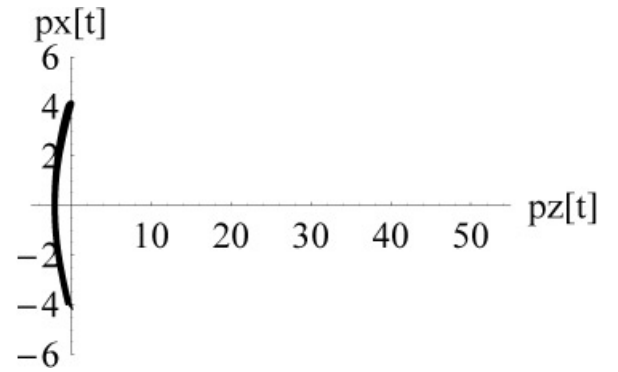

Fig. 11. Motion in the $(p_x; p_z)$ for $a_0 = 4$, $\omega_1 = 1$, $\alpha = 5\pi/6$ and $a_1 = 0.2$.

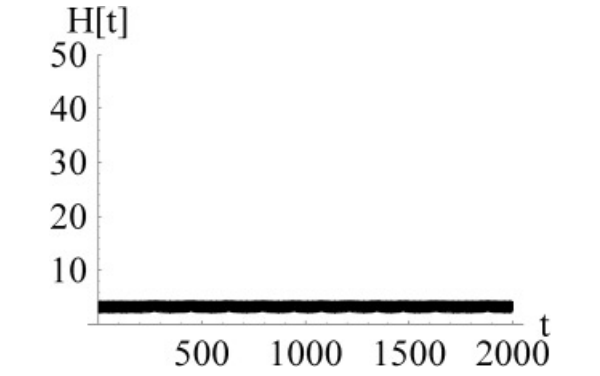

Fig. 13. Hamiltonian of the particle versus time for $a_0 = 4$, $\omega_1 = 1$, $\alpha = 5\pi/6$ and $a_1 = 0.2$.

https://doi.org/10.1017/S0263034606060320 Published online by Cambridge University Press

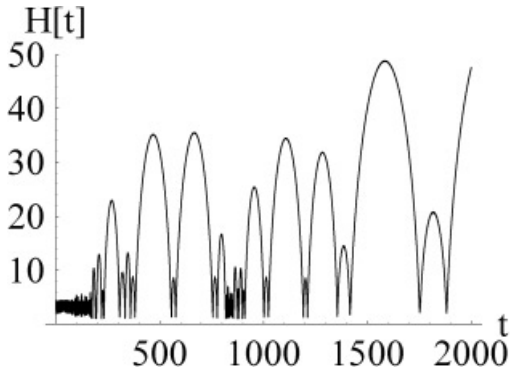

Fig. 14. Hamiltonian of the particle versus time for $a_0 = 4$, $\omega_1 = 1$, $\alpha = 5\pi/6$ and $a_1 = 0.3$.

that the Chirikov criterion is less satisfied when ω_1 is greater. Furthermore, Eq. (15) is inversely proportional with respect to ω_1.

3.4. Influence of $q = a_0/a_1$ for a given laser energy

The next simulations was performed with three waves, one with a high intensity and two perturbating waves symmetric with respect to propagation axis of the intense one. The physical parameters of the two-dimensional-simulations are $n = 10^{-2} n_c$, $\sqrt{a_0^2 + 2a_1^2} = 4$, $\omega_1 = 1$, $\tau_0 = \tau_1 = 0.62\ ps$, and $T_e = 1\ keV$, where n is the density of the plasma, τ_0 and τ_1 are the length of the two pulses and T_e is the initial temperature of the electrons. The gain is defined by:

$$Gain = \left(\frac{Ek_{3\ waves,f} - Ek_{1\ wave,f}}{Ek_{1\ wave,f}} \right) * 100, \qquad (16)$$

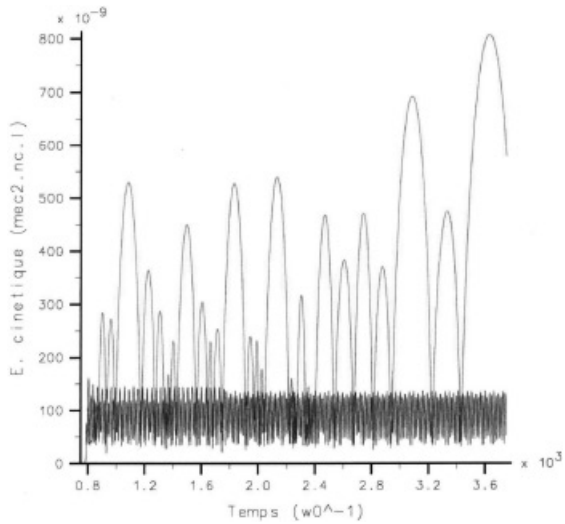

Fig. 15. Kinetic energy as a function of time computed with CALDER for two sets of parameters (see text).

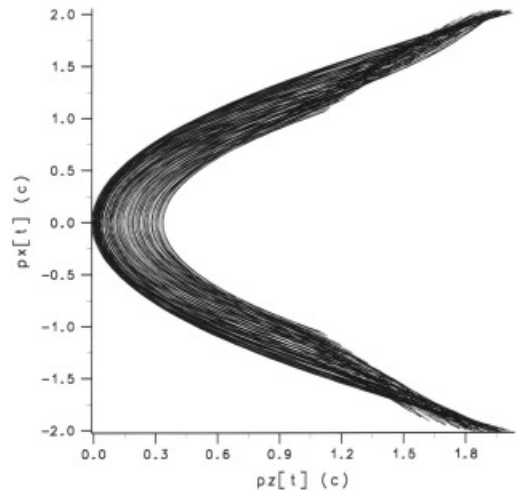

Fig. 16. Motion in the $(p_x; p_z)$ using the code CALDER with $a_0 = 2$, $\omega_1 = 1$, $\alpha = \pi$ and $a_1 = 0.1$.

where $Ek_{3\ waves,f}$ (resp. $Ek_{1\ wave,f}$) is the kinetic energy of the particles at the end of the simulation for the three wave case (resp. one wave case). The kinetic energy of the electrons is compared to the case when there is only one wave with the same laser energy (i.e., with an a equal to $\sqrt{a_0^2 + 2a_1^2}$). The relative gain and the absolute gain reach a maximum when the two counterpropagating waves amplitude ratio is 50% (Table 1). In this case, absorption is increased by more than one order of magnitude compared to the one-wave case.

3.5. Influence of the density

The simulation parameters used in the simulation are $a_0 = 3.922$, $a_1 = 0.888$ (two perturbating waves), and $T_e = 1\ keV$.

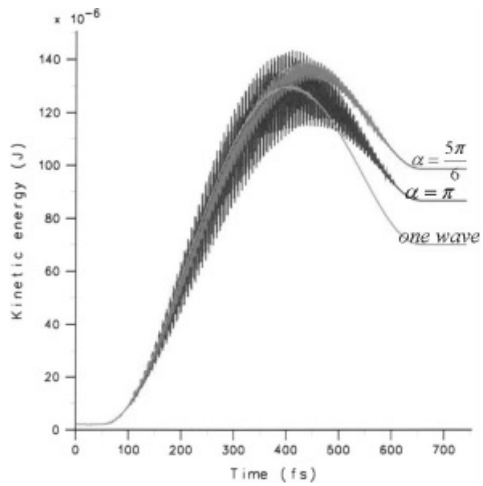

Fig. 17. Kinetic energy versus time in three cases: $\alpha = 5\pi/6$: red curve; $\alpha = \pi$: blue curve; one wave case: green curve.

https://doi.org/10.1017/S0263034606060320 Published online by Cambridge University Press

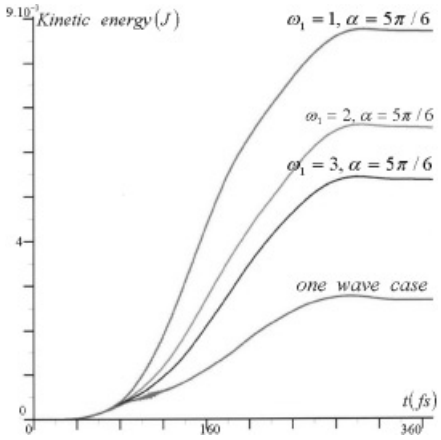

Fig. 18. Kinetic energy of the plasma.

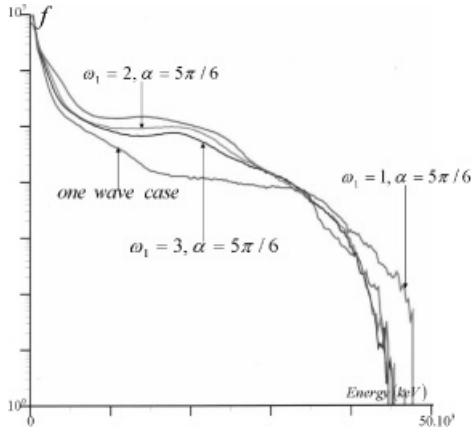

Fig. 19. Electron energy distribution.

The density is varied from $10^{-5}n_c$ to $10^{-1}n_c$. The relative gain is optimum for $n = 5\cdot10^{-2}n_c$ (*cf.* Table 2), but the absolute laser absorption is highest for $n = 10^{-1}\ n_c$ in the three waves case. It is interesting to note that the energy deposited in the plasma is larger in the three waves case at $n = 5\cdot10^{-2}\ n_c$ than in the one wave case at $n = 10^{-1}\ n_c$.

4. CONCLUSIONS

The conditions for the onset of stochastic heating was studied, in this article, within the framework of the Hamiltonian analysis. Stochastic heating was evidenced by considering single trajectories and calculating the energy of the charged particle. Furthermore, PIC code simulations with one particle highlights a chaotic behavior. PIC code simulations were also performed to confirm and optimize the occurrence of stochastic heating in more complex setups. We clearly observe that the energy deposition in the plasma is better when the system is composed of one high intensity wave and one (or two) perturbing wave. At this time, we confirm some results of Sheng *et al.* (2004) and go on for the optimization of this stochastic effect. Nevertheless, an other criterion must be found in order to prove the chaotic effect in realistic plasma. The PIC code results highlight the fact that an optimum, for the laser to plasma coupling efficiency, seems to exist for each set of experimental parameter.

REFERENCES

Bourdier, A. & Patin, D. (2005). Dynamics of a charged particle in a linearly polarized travelling wave—Hamiltonian approach to laser-matter interaction at very high intensities. *Eur. Phys. J. D* **32**, 361376.

Bourdier, A., Patin, D. & Lefebvre, E. (2005). Stochastic heating in ultra high intensity laser-plasma interaction. *Phys. D* **206**, 1–31.

Table 1. *Gain for different value of a_0/a_1. We have $Ek_{1\ wave,\ f} = 8.23\cdot10^{-4}$ (a.u.)*

a_1/a_0	1%	10%	20%	30%	50%	100%
a_0	3.999	3.960	3.849	3.682	3.265	2.309
a_1	0.039	0.396	0.769	1.104	1.632	2.309
$Ek_{3\ waves,\ f}(a.u.)$	$8.72\cdot10^{-4}$	$5.12\cdot10^{-3}$	$8.05\cdot10^{-3}$	$9.82\cdot10^{-3}$	0.011	0.011
Gain (%)	6	522	878	1093	1236	1236

Table 2. *Gain for $a_0 = 3.922$*

Density (n_c)	10^{-1}	$5\cdot10^{-2}$	10^{-2}	10^{-3}	10^{-4}	10^{-5}
$Ek_{1\ wave,\ f}(a.u.)$	0.01	$4.15\cdot10^{-3}$	$9.09\cdot10^{-4}$	$8.28\cdot10^{-5}$	$9.74\cdot10^{-6}$	$1.05\cdot10^{-6}$
$Ek_{3\ waves,\ f}(a.u.)$	0.092	0.049	$9.02\cdot10^{-3}$	$5.55\cdot10^{-4}$	$2.60\cdot10^{-5}$	$2.57\cdot10^{-6}$
Gain(%)	820	1080	892	570	166	144

https://doi.org/10.1017/S0263034606060320 Published online by Cambridge University Press

Chirikov, B. (1979). A universal instability of many-dimensional oscillator systems. *Phys. Rep.* **52**, 263–379.

Lefebvre, E., Cochet, N., Fritzler, S., Malka, V., Aléonard, M.-M., Chemin, J.-F., Darbon, S., Disdier, L., Faure, J., Fedotoff, A., Landoas, O., Malka, G., Méot, V., Morel, P., Rabec Le Gloahec, M., Rouyer, A., Rubbelynck, Ch., Tikhonchuk, V., Wrobel, R., Audebert, P. & Rousseaux, C. (2003). Electron and photon production from relativistic laser-plasma interactions. *Nucl. Fusion* **43**, 629–633.

Patin, D., Bourdier, A. & Lefebvre, E. (2005). Stochastic heating in ultra high intensity laser-plasma interaction. *Laser Part. Beams* **23**, 297–302.

Pommier, L. & Lefebvre, E. (2003). Simulations of energetic proton emission in laser-plasma interaction. *Laser Part. Beams* **21**, 573–581.

Rax, J. M. (1992). Compton harmonic resonances, stochastic instabilities, quasilinear diffusion, and collisionless damping with ultra-high-intensity laser waves. *Phys. Fluids B* **4**, 3962.

Sheng, Z.-M., Mima, K., Sentoku, Y., Jovanovic, Taguchi, T., Zhang, J. & Meyer-ter-Vehn, J. (2002). Stochastic heating and acceleration of electrons in colliding laser fields in plasma. *Phys. Rev. Lett.* **88**, 055004.

Sheng, Z.-M., Mima, K., Zhang, J. & Meyer-ter-Vehn, J. (2004). Efficient acceleration of electrons with counterpropagating intense laser pulses in vaccum and underdense plasma. *Phys. Rev. E.* **69**, 016407.

Tabor, M. (1989). *Chaos and Integrability in Nonlinear Dynamics.* New York: John Wiley and Sons.

Tajima, T., Kishimoto, Y. & Masaki, T. (2001). Cluster fusion. *Phys. Scripta* **T89**, 45–48.